Simulating electronically driven structural changes in silicon with two-temperature molecular dynamics

Robert Darkins*
London Centre for Nanotechnology, University College London, Gower Street, London, WC1E 6BT, UK

Pui-Wai Ma
UK Atomic Energy Authority, Culham Science Centre, Abingdon, Oxfordshire, OX14 3DB, UK

Samuel T. Murphy
Department of Engineering, Lancaster University, Bailrigg, Lancaster, LA1 4YM, UK

Dorothy M. Duffy
London Centre for Nanotechnology, University College London, Gower Street, London, WC1E 6BT, UK
(Dated:)

Radiation can drive the electrons in a material out of thermal equilibrium with the nuclei, producing hot, transient electronic states that modify the interatomic potential energy surface. We present a rigorous formulation of two-temperature molecular dynamics that can accommodate these electronic effects in the form of electronic-temperature-dependent force fields. Such a force field is presented for silicon which has been constructed to reproduce the *ab initio*-derived thermodynamics of the diamond phase for electronic temperatures up to 2.5 eV, as well as the structural dynamics observed experimentally under nonequilibrium conditions in the femtosecond regime. This includes nonthermal melting on a sub-picosecond timescale to a liquid-like state for electronic temperatures above ~ 1 eV. The methods presented in this paper lay a rigorous foundation for the large-scale atomistic modelling of electronically-driven structural dynamics with potential applications spanning the entire domain of radiation damage.

I. INTRODUCTION

When the electrons in a material are driven slowly relative to the electron-phonon coupling timescale, the electrons and nuclei will remain in thermal equilibrium with each other, with much of the energy supplied to the electrons translating into atomic motion. On the other hand, when electrons are driven more rapidly than they can couple with the phonons, the electrons and nuclei may be driven transiently from equilibrium, producing hot electrons and cool nuclei. Hot electronic states give rise to modified interatomic potential energy surfaces which can induce rapid phase transitions. This is referred to as a nonthermal process because it occurs before the electrons and nuclei have thermalized with each other.

Nonthermal phase transitions have been observed in multiple semiconducting and dielectric materials: Si [1–6], Ge [7, 8], GaAs [9], InSb [10], $Ge_2Sb_2Te_5$ [11], and C [12]. Band gap materials are particularly amenable to nonthermal processes because their band gaps inhibit electronic relaxation. Moreover, their atomic interactions in the ground state are determined by highly localised valence electrons whose excitation across the Fermi surface can dramatically alter the potential energy surface.

Silicon is a widely studied material in the context of strongly-driven phase transitions, both experimentally [1–6] and theoretically [13–29], where it is found to melt on a sub-picosecond timescale at high excitations. Most theoretical studies of nonthermal melting in silicon have employed *ab initio* simulation methods. However, the cost of these techniques make them unsuitable for studying large length or time scale processes such as ablation and spallation. It is within this domain of large-scale atomistic modelling of radiation damage that two-temperature molecular dynamics (2T-MD) has prevailed as the method of choice [30].

The idea of 2T-MD is to decompose the system into two subsystems: the nuclear coordinates, and a continuous scalar field representing the electronic temperature T_e throughout space. The nuclear coordinates are integrated over time using Newton's second law of motion, while the T_e field evolves according to a heat equation. The two subsystems are coupled with a thermostat that serves to thermalize them, emulating the nonadiabatic electron-phonon coupling mechanism.

Intrinsic to 2T-MD is the assumption that the electrons are always thermalized, such that a temperature is always defined. However, it is unclear how valid this approximation is. Initially, when an irradiation event takes place, the electrons will consist of thermalized low-energy electrons and a small number of high-energy electrons. In metals, the electrons thermalize to adopt a Fermi-Dirac distribution within $\sim 10-100$ fs [31], but in semiconductors thermalization can take an order of magnitude longer [3]. The electrons may, therefore, be out of quasiequilibrium during the nonthermal melting phase, in which case it would be dubious to assign an electronic temperature.

Previous theoretical studies provide limited insight

* r.darkins@ucl.ac.uk

into the significance of the electronic distribution. Most *ab initio* studies of nonthermal melting in silicon have been built on two assumptions: thermalized electrons, and the Born-Oppenheimer approximation which excludes nonadiabatic effects such as electron-phonon coupling, e.g. [16–22]. These studies do predict bond softening at high excitations but they predict melting to occur at higher excitations than expected based on experiment. More recent methods [13, 14] have avoided these two assumptions and, consequently, predicted melting at lower excitations. However, it is unclear to what extent this is attributable to the more realistic electronic distributions versus the nonadiabatic effects. Despite this uncertainty, we proceed with the assumption that the electrons instanteously thermalize, and find that the resulting model behaves in good agreement with experiment and *ab initio* simulation.

To capture the effects of electronic excitations on atomic interactions, it is necessary for the interatomic potentials to vary as a function of T_e. Deploying T_e-dependent force fields has been attempted for just four materials that we are aware of: Si [32–34], W [35, 36], Au [37], and Mo [38]. However, each one of these studies has a significant flaw.

Firstly, there is confusion regarding whether the interatomic potentials should be optimized to reproduce the energy or the free energy at finite temperatures. In the Si force field, the potential was fitted to the energy, while the other three were all fitted to the free energy. The source of confusion is that these studies have involved optimizing the interatomic potentials to fit data produced by finite-temperature density functional theory (DFT). Finite-temperature DFT ostensibly minimizes the atomic structure with respect to the free energy, specifically the grand canonical potential, which might lead one to assume the free energy should be reproduced. However, to simplify the force evaluations at the implementation level, DFT codes evaluate forces in the adiabatic limit. Minimizing the free energy in the adiabatic limit is equivalent to minimizing the energy under isothermal conditions [39, 40], and so it is the energy that should be reproduced by the interatomic potential, not the free energy.

Secondly, none of these studies deploy the T_e-dependent potentials in a way that conserves energy. Changes in the temperature give rise to changes in the potential energy, but no effort has been made to account for where this energy goes to or comes from. This concern has been raised before [41] without solution. In this paper we present the solution for correctly conserving energy in 2T-MD with T_e-dependent potentials. The solution is deceptively simple: rather than use a heat capacity precomputed for a particular phase, the heat capacity must be re-evaluated for each nuclear configuration, which can be done straightforwardly using the interatomic potentials themselves. However, expressing the heat capacity in terms of the interatomic potential places an implicit constraint on the potential which, in general, may not be satisfied for all configurations. To counter this, we introduce a potential energy correction to the Hamiltonian that is designed specifically to maintain a physically realistic heat capacity.

This new energy-conserving scheme is applied to silicon for which a new T_e-dependent potential is introduced. We do not use the existing Si potential of Shokeen et al. [32–34] because their potential is parameterized by high-degree polynomials which leads to rapid oscillations in the energy and, consequently, negative heat capacities for the crystalline phases. Futhermore, their potential gives rise to nonthermal melting at much higher energies than predicted experimentally, which our own analysis suggests is because their parameter optimization was underdetermined. In constructing a new potential, our objective was to accurately reproduce the thermodynamics of the diamond phase of silicon for a range of electronic temperatures, as well as capture the structural evolution of nonequilibrium silicon insofar as it is determined experimentally.

II. THEORY

This section presents a rigorous formulation of 2T-MD with T_e-dependent potentials, revealing how the energy of the system should be conserved. It is shown that some potentials may not be suitable for the energy-conserving scheme, for which a general-purpose many-body energy correction is introduced.

For simplicity, this paper only considers a collection of identical atoms with a uniform electronic temperature. However, the methods described may be extended straightforwardly to multi-component materials with a spatially inhomogeneous electronic subsystem in the same way as existing 2T-MD formalisms.

A. Two-temperature molecular dynamics

In our two-temperature molecular dynamics formalism, the Hamiltonian for the entire system is assumed to take the form

$$\mathcal{H} = \sum_i \frac{1}{2} m v_i^2 + U(\{\boldsymbol{R}_i\}, T_e) + \mathcal{H}_e(T_e), \qquad (1)$$

where m is the atomic mass, v_i are the atomic velocities, $U(\{\boldsymbol{R}_i\}, T_e)$ is a T_e-dependent interatomic potential, $\{\boldsymbol{R}_i\}$ are the nuclear degrees of freedom, and $\mathcal{H}_e$ is the Hamiltonian for the electronic subsystem. We need not specify the functional form of $\mathcal{H}_e$ but assume its state to be solely determined by the electronic temperature T_e.

By parameterizing the electronic state with just a temperature, we have implicitly deployed the Born-Oppenheimer approximation and assumed instantaneous thermalization of the electrons in response to nuclear motion, which gives rise to an adiabatic potential energy surface. Since electron-phonon coupling is a perturbative

correction to this adiabatic approximation, it does not naturally arise from the Hamiltonian. Instead, electron-phonon coupling may be incorporated via the Langevin equation of motion, which treats the nuclei as experiencing fluctuation forces from the electronic thermal reservoir,

$$m\frac{d\boldsymbol{v}_i}{dt} = -\frac{\partial U}{\partial \boldsymbol{R}_i} - \gamma \boldsymbol{v}_i + \boldsymbol{f}_i, \tag{2}$$

where γ is a damping parameter and $\boldsymbol{f}_i$ is a delta-correlated stochastic force that satisfies the conditions $\langle \boldsymbol{f}_i \rangle = 0$ and $\langle f_{i\alpha}(t) f_{j\beta}(t') \rangle = \mu \delta_{ij} \delta_{\alpha\beta} \delta(t - t')$. It follows from the fluctuation-dissipation theorem [42–44] that, when the electrons and nuclei are in thermal equilibrium with each other, $\mu = 2\gamma k_B T_e$, where k_B is Boltzmann's constant. As with previous work [45, 46], we make the assumption that this relation holds true even out of equilibrium. The damping parameter γ may then be chosen such that the electronic and nuclear temperatures converge on a desired timescale after being driven from equilibrium.

It follows from the Hamiltonian in Eq. (1) that the time-derivative for the total energy of the system will be

$$\frac{dE}{dt} = \sum_i \boldsymbol{v}_i \cdot (-\gamma \boldsymbol{v}_i + \boldsymbol{f}_i) + \left(\frac{\partial U}{\partial T_e} + \frac{dE_e}{dT_e} \right) \frac{dT_e}{dt}, \tag{3}$$

where E_e is the energy of the electronic subsystem, and we have substituted Eq. (2). The rate at which the energy of the system changes will equal the rate at which energy is dumped into the system by an external heat source Q, and so Eq. (3) begets the heat equation

$$C_e \frac{dT_e}{dt} = -\sum_i \boldsymbol{v}_i \cdot (-\gamma \boldsymbol{v}_i + \boldsymbol{f}_i) + Q, \tag{4}$$

where the first term on the right-hand side is to be interpreted as the electron-phonon coupling power, and the electronic heat capacity is

$$C_e = \frac{dE_e}{dT_e} + \frac{\partial U}{\partial T_e}. \tag{5}$$

The heat source Q only measures the power of the absorbed energy over time. It is indifferent to the nature of the source, whether laser or swift heavy ion, and to the mechanism of absorption. Note that, to model a spatially inhomogeneous electronic subsystem with thermal conductivity κ, a diffusion flux $\nabla \cdot \kappa \nabla T_e$ should be added to Eq. (4).

At this stage, Eqs. (1), (2), (4), and (5) provide a T_e-dependent 2T-MD formalism that conserves energy. Where it differs from previous applications of 2T-MD, which fail to conserve energy, is that the heat capacity C_e has an explicit $\partial U/\partial T_e$ component, making it a function of both T_e and the nuclear configuration $\{\boldsymbol{R}_i\}$, rather than a function of T_e alone.

As is common practice, we replace the electron-phonon coupling power in Eq. (4) with its ensemble average, which can be derived by applying the Furutsu-Novikov theorem to the term containing the stochastic force [47–49], resulting in

$$\left\langle -\sum_i \boldsymbol{v}_i \cdot (-\gamma \boldsymbol{v}_i + \boldsymbol{f}_i) \right\rangle = \frac{3\gamma k_B N}{m} (T_n - T_e), \tag{6}$$

where T_n is the nuclear temperature and N the number of atoms. Phillips et al. [50] have cautioned against this substitution since it introduces energy drift into the system. However, for the large system sizes used in the present work, we found the drift to be indistinguishable from that produced by the symplectic integrator. Moreover, using the ensemble average has the advantage that the heat equation (4) may be numerically integrated more efficiently with use of Suzuki-Trotter decomposition [51].

Some previous efforts [26, 27, 41, 52] to model silicon with a two-temperature model have been based on the framework of van Driel [23] which parameterizes the system with the carrier density, in addition to the usual electronic and nuclear temperatures. The carrier density evolves according to a separate differential equation that captures carrier generation, diffusion, and recombination. This approach has the advantage that the electronic heat capacity may be expressed as a function of the carrier density, and the optical properties of the material are more straightforwardly accounted for by using the carrier density to attenuate the radiation intensity as it passes through the material. However, as previously noted [30], explicitly including a term for the carrier density is superfluous since the carrier density has a one-to-one relationship with the electronic temperature under (quasi)equilibrium conditions. It follows that any function of the carrier density may instead be written as a function of electronic temperature. Moreover, expressing the electronic heat capacity as a function of the carrier density fails to give rise to a configuration-dependence, and so such a model is ill-suited to modelling phase transitions. In any case, we do not model radiation attenuation in this work and so do not require an explicit carrier density.

B. On-the-fly energy correction

One of the challenges with deploying the energy-conserving formalism described above is that it is necessary for the heat capacity C_e to always be positive, as one would expect on purely physical grounds. Even more strictly, the heat capacity should not be able to become arbitrarily close to zero for any configuration or electronic temperature. It is therefore necessary for the heat capacity to have a finite lower bound $\epsilon(T_e)$ that holds for all nuclear configurations. This gives rise to the following constraint on the potential U:

$$\min_{\{\boldsymbol{R}_i\}} \frac{\partial U}{\partial T_e}(\{\boldsymbol{R}_i\}, T_e) \geq \epsilon(T_e) - \frac{dE_e}{dT_e}(T_e). \tag{7}$$

In general, a T_e-dependent potential will not satisfy this constraint and so it must be explicitly imposed. Typically, this will not be possible through careful parameterization alone, but will instead demand changes to the functional form of the potential. To illustrate the need for such an intervention, consider a simple T_e-dependent pairwise potential of the form $U = \sum_{i<j} A(T_e)\phi_R(r_{ij}) - B(T_e)\phi_A(r_{ij})$, where ϕ_R (ϕ_A) are repulsive (attractive) functions of the atomic separations r_{ij}. The T_e-dependence of A and B might reasonably exhibit, for some T_e, the property $dA/dT_e = 0$ and $dB/dT_e > 0$. In this case, given an arbitrary number of atoms packed arbitrarily densely, one could make the per-atom value of $\partial U/\partial T_e$ arbitrarily negative, and thus no minimum for $\partial U/\partial T_e$ would even exist. But this is not just a hypothetical problem that arises for extreme configurations. Rather, the derivative $\partial U/\partial T_e$ may become too negative for entirely plausible configurations, as will be shown to be the case for the silicon potential introduced later in this paper.

To understand why this problem should arise at all, note that interatomic potential functional forms, and their parameterizations, are generally constructed to reproduce the potential energy surface of materials near to crystalline phases. It is not surprising then that they should behave unphysically for, say, certain highly-dense amorphous configurations with highly excited electrons.

In the absence of more accurate many-body potentials, we resolve the issue by introducing a general many-body energy correction $W(\{\boldsymbol{R}_i\}, T_e)$ that is added to the Hamiltonian of Eq. (1). The correction is general in the sense that it is evaluated numerically on-the-fly at each integration time-step and works for any potential U. The correction takes the form

$$W(\{\boldsymbol{R}_i\}, T_e) = \int_0^{T_e} w(C_e(\{\boldsymbol{R}_i\}, T_e'), \epsilon(T_e'))\, dT_e', \quad (8)$$

where w is specifically constructed to satisfy

$$C_e + w(C_e, \epsilon) \geq \epsilon. \quad (9)$$

This correction leads to the heat capacity C_e in the heat equation (4) being replaced with $C_e + w$ which is now guaranteed to be not less than ϵ, per Eq. (9). It also gives rise to auxiliary atomic forces which depend on the forces from the interatomic potential U,

$$-\frac{\partial W}{\partial \boldsymbol{R}_k} = -\frac{\partial w}{\partial C_e}\frac{\partial U}{\partial \boldsymbol{R}_k} + \int_0^{T_e} \frac{\partial^2 w}{\partial T_e' \partial C_e}\frac{\partial U}{\partial \boldsymbol{R}_k}\, dT_e'. \quad (10)$$

The derivation is provided in Appendix A where it has been assumed that $\partial U/\partial T_e(T_e = 0) \equiv 0$.

The precise functional form of w is of little significance, but it should be twice-differentiable and satisfy

$$w(C_e \leq 0, \epsilon) = \epsilon - C_e, \quad (11)$$

$$w(C_e \geq f\epsilon, \epsilon) = 0, \quad (12)$$

$$-1 \leq \frac{\partial w}{\partial C_e}(0 < C_e < f\epsilon, \epsilon) \leq 0, \quad (13)$$

for some constant f in the interval

$$1 < f \leq \min_{T_e} \frac{1}{\epsilon(T_e)}\frac{dE_e}{dT_e}(T_e). \quad (14)$$

The value of f determines how hard or soft the energy correction is as C_e approaches the lower bound. In the limit $f \to 1^+$, the corrective energy becomes hard, giving rise to infinitely large forces. It is bounded from above to ensure that $W = 0$ for the isolated system. A suitable expression for w is provided in Appendix A which has an f value of 2.

The action of the auxiliary forces in Eq. (10) may be understood as follows: For a given configuration, if T_e changes such that C_e becomes too close to ϵ, or even smaller than ϵ, then the forces $-\partial U(T_e)/\partial \boldsymbol{R}_k$ are smoothly switched off and replaced with an average of forces that would act at lower electronic temperatures in regions where C_e is above ϵ. Essentially, the energy landscape is perturbed towards its form at lower electronic temperatures where the potential is better behaved.

To summarize, any T_e-dependent potential U may be safely deployed in an energy-conserving two-temperature molecular dynamics scheme without further modification, so long as the energy correction W described above is incorporated. And while it is true that this correction is *ad hoc* with the purpose of producing more physically realistic heat capacities, its use can be further justified with a few observations: Firstly, the heat capacity will only become too small if the potential energy U decreases too rapidly. The correction therefore gives rise to more physically realistic potential energies $U + W$ than produced by U alone. Secondly, the correction will typically only be activated under highly nonequilibrium conditions for which the true structure and dynamics are seldom known. Thirdly, interatomic potentials are themselves approximations, and so introducing an approximate correction is not antithetical to the molecular mechanics enterprise. Finally, the alternative approaches to satisfying Eq. (7) appear to be highly non-trivial, although future research may reveal better solutions.

It is worth lingering briefly on the implementation details for this energy correction since it effectively requires that, at each integration time-step, the energy U and all of the atomic forces $-\partial U/\partial \boldsymbol{R}_k$ are known at all electronic temperatures ranging from 0 K up to the prevailing temperature T_e. At first glance, one might expect this to incur a tremendous computational burden, but there exist optimizations; in particular, the energy and atomic forces do need to be evaluated over a discrete set of electronic temperatures, but this can be done with little additional cost if evaluated concurrently such that the T_e-independent parts of the force field are not re-evaluated for each temperature. The energies and forces may then be obtained over a continuous temperature range through cubic spline interpolation. In our particular code implementation, a small energy drift still exists due to numerical errors, but was found to be on the order of 0.1% of the energy dumped into the system by the external heat

source.

III. T_e-DEPENDENT SILICON FORCE FIELD

In this section, a new T_e-dependent force field for silicon is presented. It is described in enough detail to be understood, but the complete functional form and parameterization is provided in Appendix B.

The MOD [53] version of the Tersoff potential [54] for silicon is well-established and known [55, 56] to reasonably reproduce the experimental cohesive energy, crystalline and liquid heat capacities, elasticity properties, latent heat of melting, and melting temperature of the diamond phase, as well as *ab initio* defect energies. Its functional form is

$$U = \frac{1}{2}\sum_{i\neq j} f_c(r_{ij})(Ae^{-\lambda_1 r_{ij}} - b_{ij}Be^{-\lambda_2 r_{ij}}), \tag{15}$$

where r_{ij} is the ij atomic distance and f_c is a cutoff function which smoothly switches off interactions between the cutoff radii R_1 and R_2. There is also a bond order b_{ij} which makes U a many-body potential and takes the form

$$b_{ij} = (1+\zeta_{ij}^{\eta})^{-\delta}, \tag{16}$$

$$\zeta_{ij} = \sum_{k\neq i,j} f_c(r_{ik})g(\theta_{ijk})e^{\alpha(r_{ij}-r_{ik})^{\beta}}, \tag{17}$$

where θ_{ijk} is the angle between the ij and ik bonds, and the angle-dependence $g(\theta_{ijk})$ serves to emulate directional bonding. All other terms are parameters.

In this work, the same functional form for the ground state ($T_e = 0$) is adopted. To introduce a T_e-dependence into the potential, the parameters A and B are assumed to vary with T_e and will thus need to be optimized over a range of different electronic temperatures, while all of the other parameters are held constant. However, while scaling A and B will reproduce the energy in the crystal phase, it alone will not reduce the activation barriers between the diamond and amorphous phases, and so a further modification is required to induce nonthermal melting.

Observe that the electronic structure in the ground state of the diamond silicon phase consists of sp^3 hybridized orbitals which are responsible for the tetrahedral bond geometry. When the electrons become excited, this bond directionality will diminish, thus destabilizing the crystal structure and inducing the phase transition. To incorporate the softening of the bond directions into the potential, the bond-angle dependence $g(\theta)$ in Eq. (17) is substituted with the function

$$g(\theta_{ijk}) \leftarrow g(\theta_{ijk}) - \Lambda(g(\theta_{ijk}) - g_0, \lambda(T_e)), \tag{18}$$

where $g_0 = g(\cos^{-1}(-1/3))$ is the value of g for tetrahedral geometry, and the Λ function is constructed such that $\Lambda(|\Delta g| \gg \lambda, \lambda) = \mathrm{sgn}(\Delta g)\lambda$ and $\Lambda(|\Delta g| \ll \lambda, \lambda) = \Delta g$, with a smooth variation between these two bounds.

The purpose of this modification is to shift $g(\theta)$ closer to the constant g_0 by an amount no greater than $\lambda(T_e)$, and to do so in a differentiable manner. To clarify, Figure 1(d) shows a plot of $g(\theta) - \Lambda(g(\theta) - g_0, \lambda)$ for $\lambda = 0$ (in which case $\Lambda = 0$), 0.2, and 0.4. The consequence is that, as λ increases from 0 to its finite value at higher electronic temperatures, the angle dependence within the potential flattens out in the region where $g(\theta) = g_0$. This amounts to a softening of the directionality of the bonding which helps to destabilize the diamond structure and induce rapid nonthermal melting.

A. Parameter fitting

Following Shokeen et al. [33], the ground state parameters are chosen to match those of the MOD potential, except the cutoff radii are increased to $R_1 = 3.1$ and $R_2 = 3.4$ Å and the α parameter is adjusted to a value of 1.90 to improve the melting temperature.

As described in the previous section, the T_e-dependent parameters in our potential are $A(T_e)$, $B(T_e)$, and $\lambda(T_e)$. In addition to these, the Langevin damping constant γ and the lower bound on the heat capacity $\epsilon(T_e)$ are also required. In the diamond phase, where the bonds exhibit perfect tetrahedral geometry, λ is designed to have no effect on the potential. The parameters A and B may therefore be optimized for the diamond phase independently of λ.

To this end, *ab initio* methods were used to compute the potential U_{ab} for the diamond phase over the range $0 \leq T_e \leq 2.5$ eV in increments of 0.05 eV. This involved two steps: Firstly, for each T_e, the energy $E_{\mathrm{ab}}(\{\boldsymbol{R}_i\}, T_e)$ was computed for atomic volumes ranging from 12 to 43 Å^3. And secondly, for the same temperature range, the energy of the isolated system, $E^0_{\mathrm{ab}}(T_e)$, where the atoms are effectively separated to infinity, was computed. The *ab initio* potential may then be computed as $U_{\mathrm{ab}}(\{\boldsymbol{R}_i\}, T_e) = E_{\mathrm{ab}}(\{\boldsymbol{R}_i\}, T_e) - E^0_{\mathrm{ab}}(T_e)$, while the energy of the electronic subsystem is $E_e(T_e) = E^0_{\mathrm{ab}}(T_e) - E^0_{\mathrm{ab}}(0)$. This necessarily fulfils the requirement that when the system is isolated at $T_e = 0$, both U_{ab} and E_e will equal zero.

Recall that the potential U has already been chosen for the ground state. It would be unlikely for this U to perfectly align with the *ab initio* potential U_{ab} at $T_e = 0$. The parameters A and B are therefore instead fitted such that $U(\{\boldsymbol{R}_i\}, T_e)$ reproduces $U_{\mathrm{ab}}(\{\boldsymbol{R}_i\}, T_e) + U(\{\boldsymbol{R}_i\}, 0) - U_{\mathrm{ab}}(\{\boldsymbol{R}_i\}, 0)$. This way our ground state potential is preserved while the T_e-dependence obtained from the *ab initio* calculations is reproduced.

The *ab initio* calculations were performed using the Vienna Ab initio Simulation Package (VASP) [57–60]. The diamond crystal was represented with two atoms per unit cell, with four valence electrons per atom. The plane wave cutoff energy was 400 eV with $21 \times 21 \times 21$ k-points used for the crystal phase. The isolated system was modelled with a single atom in a $9 \times 9 \times 9$ Å

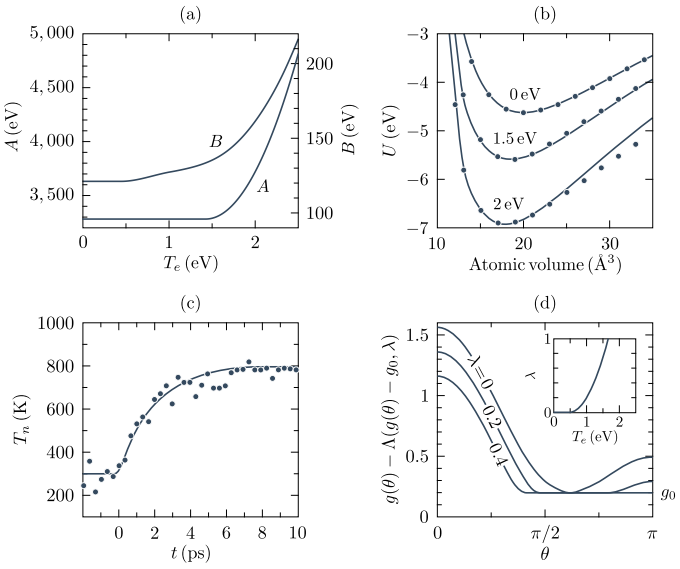

FIG. 1: (a) The dependence of the A and B force field parameters on electronic temperature T_e. (b) The interatomic potential U for a range of atomic volumes in the diamond phase, and for $T_e = 0$, 1.5, and 2 eV. The lines are the 2T-MD interatomic potential while the circles are the *ab initio* calculations. (c) The evolution of the nuclear temperature T_n in response to a low-fluence excitation at $t = 0$. The line is the 2T-MD calculation, the circles are experimental data points [1]. (d) The modified angle-dependence for $\lambda = 0, 0.2, 0.4$, corresponding to a weakening of bond directionality. The inset shows the dependence of λ on electronic temperature.

box and only the Γ-point sampled. An electronic temperature is introduced by treating the electronic states as distributed according to the Fermi-Dirac distribution [61]. We used the M06-L [62] exchange-correlation functional which produces a band gap of 1.12 eV [63] in good agreement with the experimental band gap of 1.11 eV [64]. By contrast, the GGA-PBE [65] functional produces a band gap of 0.75 eV, while the hybrid functional is an order of magnitude slower to execute than M06-L.

The resulting T_e-dependence of A and B is shown in Figure 1(a). At low T_e, both parameters are constant, with a steady increase in B as the temperature increases, followed by a rapid increase in both A and B at high temperatures. The result is a potential energy surface that deepens with increasing electronic temperature, with a minor reduction in the equilibrium atomic volume, as shown in Figure 1(b). The deepening of the potential is presumably a result of the electrons becoming less localized, leading to the positively-charged nuclei being exposed to a greater negative charge.

Before optimizing the λ function, it is necessary to obtain the Langevin damping parameter γ which characterizes the electron-phonon coupling rate. For this we turn to the experimental data of Harb et al. [1, 2] who measured the structural response of silicon nanofilms to ultrafast photoexcitations. The relevant details of their experiment along with our approach to modelling it can be found in Appendix C. In one particular experiment, the nuclear temperature was recorded with femtosecond resolution following a laser irradiation event with an absorbed fluence of $\Phi = 5.6$ mJ/cm^2. This fluence is below the damage threshold and excites the lattice thermally, and so the parameter λ may be fixed to zero at this stage. The damping parameter γ could then be optimized such that the nuclear temperature evolves over the same timescale as seen experimentally. Excellent agreement was achieved with a value of $\gamma = 1$ g/mol/ps, as shown in Figure 1(c).

The next parameter to optimize is the function $\lambda(T_e)$, which is responsible for inducing rapid nonthermal melting. There is currently not enough information available to optimize λ for each individual temperature. Instead, it is constructed somewhat arbitrarily to satisfy certain constraints. In the ground state λ is necessarily 0, but to establish its value in excited states we return to the experimental data of Harb et al. (cf. Appendix C). Experimentally, a damage threshold was observed at an absorbed fluence of $\Phi = 6$ mJ/cm^2, below which the Bragg peaks decay in accordance with the Debye-Waller factor. One might therefore predict that the shape of the potential begins to change around the damage threshold. Based on the value of γ previously obtained, the damage threshold in our model was found to correspond to a peak electronic temperature of 0.45 eV. It is at this temperature, therefore, that λ will begin to increase from 0. Another data point is that above an absorbed fluence of approximately $\Phi = 30$ mJ/cm^2 the crystal melts nonthermally in under a picosecond. In our model it is found that $\lambda \geq 0.2$ is sufficient to induce rapid melting, and that the reported fluence corresponds to a peak electronic temperature of 1 eV. In summary, the parameter λ should satisfy $\lambda(T_e \leq 0.45\,\text{eV}) = 0$ and pass through $\lambda(1\,\text{eV}) = 0.2$. With use of a polynomial, a smooth curve satisfying these conditions was constructed, and it can be seen in the inset of Figure 1(d).

The final function to be optimized is $\epsilon(T_e)$ which imposes a lower bound on the electronic heat capacities. Based on the shape of the w function that we employed, ϵ must satisfy the constraint $\epsilon(T_e) \leq \frac{1}{2}\frac{dE_e}{dT_e}(T_e)$, per Eq. (14). It should also be small enough that $C_e \geq 2\epsilon$ (and thus $W = 0$ per Eq. (12)) for the diamond crystal structures for which U was optimized, since U was tacitly optimized under the assumption that $W = 0$. To satisfy these constraints and estimate a lower bound on the heat capacity, the minimum value for C_e was computed for each temperature from the *ab initio* data $\partial E_{\text{ab}}/\partial T_e$ over the range of atomic volumes sampled, and the results were halved. It was found that $\epsilon(T_e) = \frac{1}{7}\frac{dE_e}{dT_e}(T_e)$ provided a reasonable estimate while satisfying the constraints specified.

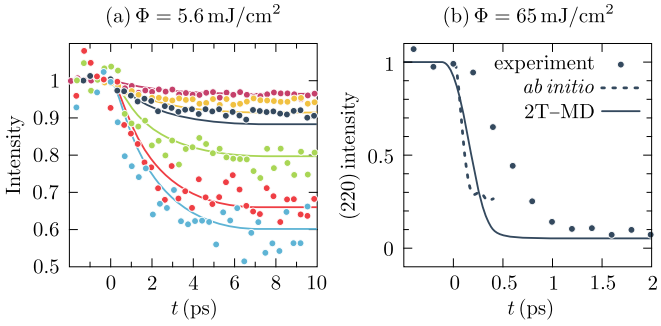

FIG. 2: (a) Several normalized Bragg peaks decaying in response to a low-fluence laser pulse at $t = 0$. The lines are predicted from 2T-MD while the circles are experimental measurements [1]. From top to bottom, the peaks are: (111), (220), (311), (331), (531), (620). (b) The normalized response of the (220) Bragg peak to a high-fluence laser pulse that nonthermally melts the crystal. The *ab initio* data (dashed line) was taken from [13] and the experimental data (circles) from [2].

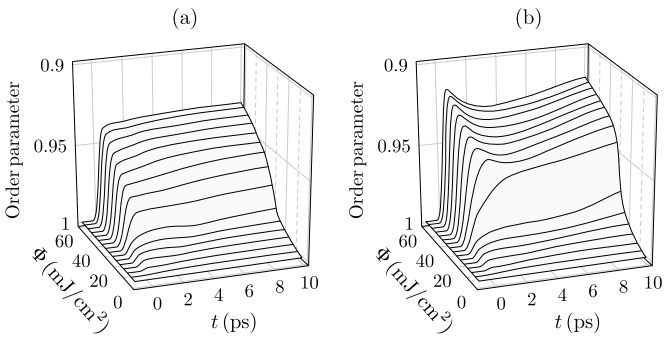

FIG. 3: The evolution of the centrosymmetry order parameter in response to an ultrafast laser pulse at $t = 0$ for a range of absorbed fluences for simulations that (a) conserve energy, and (b) do not conserve energy. A larger value corresponds to more order (centrosymmetry), but note the inverted axis.

IV. DISCUSSION

Having presented a new T_e-dependent force field for silicon (Section III), and a formalism for conserving energy (Section II), this section answers the following questions: How does the predicted structural evolution of irradiated silicon compare to experiment? How does the system evolve during a phase transition? How is energy conserved and how do the results compare to analogous simulations that fail to conserve energy? And what effect does the on-the-fly energy correction have on the dynamics of the system?

The structural evolution of silicon in response to electronic excitation displays two distinct domains: thermal agitation at low excitations, and rapid melting at high excitations that sufficiently modify the potential energy surface. In the experiments of Harb et al. (cf. Appendix C) the Bragg peak response was measured for silicon nanofilms irradiated with an ultrafast laser pulse across both the low and high fluence domains. Figure 2(a) shows the evolution of several normalized Bragg peaks for a low absorbed fluence of $\Phi = 5.6$ mJ/cm^2, as predicted by our model (lines) along with the corresponding experimental measurements (circles). There is generally very good agreement.

The experiments also determined that above a fluence of approximately 30 mJ/cm^2, the crystal structure melts rapidly. Our force field was constructed specifically to satisfy this condition, and the evolution of the (220) peak at a fluence of 65 mJ/cm^2 is shown (solid line) in Figure 2(b) along with the experimental measurements (circle). Also shown is the (220) peak decay computed with real-time time-dependent density functional theory by Lian et al. [13] for the same level of excitation. The peak rapidly decays within a picosecond in all cases, although the simulations both predict a quicker collapse of the structure than the experimental data would imply. However, in the experiment, the optical pump and the probe have overlapping distributions such that the probe is really measuring the average decay over a range of fluences, with the reported fluence being the average. This could explain the observed discrepancy between experiment and simulation, and would be supported by earlier experiments that found the crystal structure to melt within only 150 fs [5].

To see how the system evolves over time for a broad range of fluences, simulations of the ultrafast irradiation of nanofilms (as described in Appendix C) were performed for absorbed fluences $0 \leq \Phi \leq 60$ mJ/cm^2 and over a time interval $-1 \leq t \leq 10$ ps, where the excitation event occurs at $t = 0$. The degree of order in the atomic structure over this (Φ, t)-space can be quantified with the centrosymmetry order parameter [26] as shown

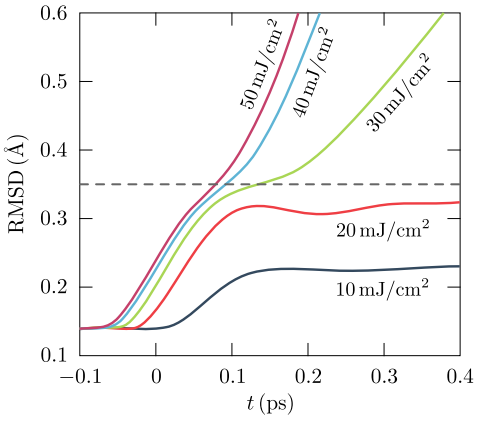

FIG. 4: The root-mean-square deviation of the atomic positions in response to a laser pulse at $t = 0$ with the absorbed fluence labelled.

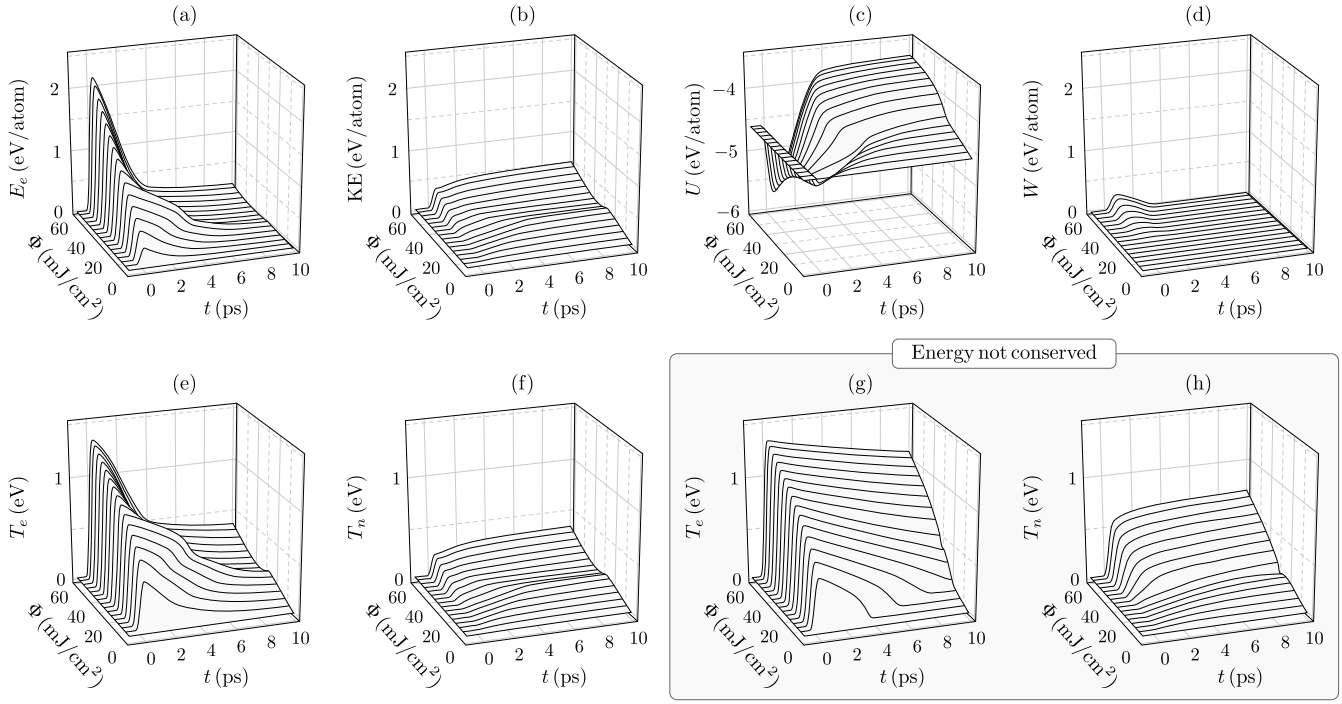

FIG. 5: (a)-(d) The time evolution of the four Hamiltonian components in response to an ultrafast laser pulse at $t = 0$ for a range of absorbed fluences Φ, as well as the (e) electronic temperature and (f) nuclear temperature. (g) and (h) are the same as (e) and (f), respectively, but for simulations that do not conserve energy.

in Figure 3(a). When modelling phase transitions with a femtosecond temporal resolution, it is not practical to define a hard threshold that demarcates the crystalline phase from the melt. Nevertheless, a qualitative change in the order parameter can be seen to occur in the vicinity of ~ 30 mJ/cm^2, indicative of a phase transition, as expected. Further information about the melting process can be gleaned from the root-mean-square deviation (RMSD) of the atomic positions over time, shown in Figure 4. For the fluences that do not give rise to nonthermal melting ($\Phi < 30$ mJ/cm^2), the RMSD is confined to approximately 0.35 Å of deviation, which is the same bound estimated from nonadiabatic *ab initio* simulation [13]. The nonlinearity of the RMSD in the initial ~ 150 fs after the excitation indicates that a small activation barrier to melting remains, in general agreement with Refs [2, 13]. The steady and rapid rise of the RMSD after the structure has melted is indicative of a liquid-like phase rather than an amorphous solid, as previously established to be true [2, 13, 14].

Having deployed an energy-conserving 2T-MD scheme, it is insightful to see how the individual components of the Hamiltonian evolve in response to an electronic excitation. Figure 5 shows this for (a) the electronic energy E_e, (b) the nuclear kinetic energy, (c) the interatomic potential energy U, and (d) the on-the-fly correction W. Also shown is (e) the electronic temperature T_e and (f) the nuclear temperature T_n. The initial excitation produces a jump in the electronic energy E_e and temperature T_e, as well as a drop in the potential energy U due to its T_e-dependence. This excitation is attenuated by the electron-phonon coupling which leads to an increase in the nuclear kinetic energy. As previously described, for the fluence range $\Phi \gtrsim 30$ mJ/cm^2, the change in the potential energy surface leads to the formation of a disordered liquid-like phase. This disordering of the configuration results in a significant decline in the heat capacity C_e, as evidenced by the more rapid decline in E_e than T_e. This means that, while the electronic temperature remains high, the energy content stored in the electrons has greatly diminished due to the disordering of the atomic structure. The electronic energy is therefore depleted much more rapidly by its exchange with the phonons, leading to a rapid drop in T_e at high fluences and an equilibration with the nuclei within several picoseconds. Note that an initial increase of the fluence across the ~ 30 mJ/cm^2 threshold causes a decrease in the nuclear temperature by up to 400 K. This non-monotonicity of T_n with respect to Φ is a result of the structure melting to form a higher-energy configuration which necessarily leads to a decline in the nuclear velocities. The energy component W will be discussed further below.

It is interesting to compare the evolution of the electronic and nuclear temperatures in our model to those produced using the same method as previous papers which fail to conserve energy. This non-conserving approach involves precomputing the heat capacity $C_e(T_e)$ for a zero-temperature crystal phase, in our case the di-

amond phase, and also neglects the W correction. The resulting temperature evolution is shown in Figures 5(g) and (h) and should be compared with the respective plots in Figures 5(e) and (f) for which the energy is correctly conserved. Since the heat capacity is not a function of the configuration in the non-conserving approach, it is unperturbed by the phase transition, displaying a steady increase in T_e with increasing fluence, and a correspondingly large increase in the nuclear temperature. Even after 10 ps the two subsystems have yet to equilibrate, and yet the nuclear temperature has reached twice its value in the conserved system. Taking care to correctly conserve the energy, therefore, has significant consequence for the evolution of the system.

In Section IIB, a many-body energy correction W was introduced to the Hamiltonian to compensate for the fact that certain configurations produce, at certain electronic temperatures, heat capacities C_e that are unphysically small or even negative. This correction is indeed activated for our potential, as shown in Figure 5(d). Specifically, it is activated when the structure is highly disordered and the electronic temperature sufficiently elevated. The magnitude of W is visibly small, on the order of one-tenth of the energy dumped into the system by the laser, but it nevertheless has some observable dynamical effects. Figure 3 shows the evolution of the centrosymmetry order parameter for (a) when energy is conserved and the on-the-fly energy correction enabled, and (b) when the energy is not conserved and the correction disabled. In the latter case, the order parameter initially spikes as the large T_e flattens the potential energy surface, permitting the exploration of highly non-centrosymmetric configurations. As the electronic temperature begins to drop, the atomic forces are partially restored, driving the configuration back towards increased centrosymmetry. Thereafter, the nuclei heat up through electron-phonon coupling, providing enough energy for the structure to access regions of greater disorder (less centrosymmetry). This initial spike is not seen when the on-the-fly correction is enabled, because W increases the energy cost of such highly disordered (highly non-centrosymmetric) structures, making them inaccessible at the prevailing nuclear temperatures.

The activation of W for these highly non-centrosymmetric structures indicates that the potential energy U declines too rapidly with respect to T_e for those particular structures. The fact that the functional form and parameterization of our interatomic potential should exhibit an unphysical drop in U for these particular structures is not obvious *a priori*, and demonstrates the expediency of an on-the-fly correction.

V. CONCLUSIONS

When radiation is delivered on a femtosecond timescale, it can drive the electrons and nuclei out of equilibrium, producing hot electrons and cool nuclei. The hot electrons modify the potential energy surface and can induce rapid phase transitions. Such electronic effects can be incorporated into two-temperature molecular simulation with the use of electronic-temperature-dependent force fields. However, previous attempts to deploy such force fields have failed to conserve energy.

In this paper, a rigorous formulation for two-temperature molecular dynamics with electronic-temperature-dependent force fields has been presented, revealing that the interatomic potential energy forms a component of the electronic heat capacity, and that evaluating the heat capacity as a function of the atomic configuration leads to conserved energy. It transpires, however, that an energy-conserving scheme imposes a constraint on the interatomic potential which, in general, may not be satisfied. To resolve this, we advocate for the use of an on-the-fly correction to the Hamiltonian that introduces an energy penalty where necessary so as to retain a physical electronic heat capacity.

Within this energy-conserving framework, a new semi-empirical force field has been derived for silicon. The force field was optimized to reproduce *ab initio* data in the diamond phase, and to melt to form a liquid-like phase at the same excitation observed experimentally. The melting is induced by relaxing the directionality of the bonding, allowing the centrosymmetry of the structure to collapse.

The new force field will enable, for the first time, the accurate simulation of nonthermal processes in strongly-driven silicon systems on large length and time scales. More generally, the new formalism developed in this paper lays a foundation for the study of ultrafast dynamics in response to extreme irradiation conditions over large length and time scales.

ACKNOWLEDGMENTS

RD, STM, and DMD acknowledge funding from the Leverhulme Trust under Grant No. RPG-2013-331. PWM has worked within the framework of the EUROfusion Consortium and has received funding from the Euratom research and training programme 2014-2018 under Grant Agreements No. 633053 and No. 755039, and has been partially funded by the RCUK Energy Programme (Grant No. EP/P012450/1). The views and opinions expressed herein do not necessarily reflect those of the European Commission.

Appendix A: On-the-fly energy correction: functional form and force derivation

In this work, the Hamiltonian contains a many-body energy correction W which is expressed in terms of its T_e-derivative w. As described in Section II B, the precise functional form of w is of little significance, but it must be twice-differentiable and satisfy the conditions set out

in Eqs. (11)-(13). In this work we employ the following function:

$$w(C_e, \epsilon > 0) = \begin{cases} \epsilon - C_e & C_e \leq 0 \\ \epsilon - \frac{9}{8}\frac{\epsilon}{\pi}\sin\left(\frac{\pi}{2}\frac{C_e}{\epsilon}\right) + \frac{1}{8}\frac{\epsilon}{3\pi}\sin\left(\frac{3\pi}{2}\frac{C_e}{\epsilon}\right) - \frac{1}{2}C_e & 0 < C_e < 2\epsilon \\ 0 & C_e \geq 2\epsilon \end{cases}, \tag{A1}$$

which has a corresponding f value of 2.

The auxiliary forces that arise from the energy correction W are given in Eq. (10). Here we provide a derivation that follows on from Eq. (8):

$$-\frac{\partial W}{\partial \boldsymbol{R}_k}(\{\boldsymbol{R}_i\}, T_e) = -\int_0^{T_e} \frac{\partial w}{\partial \boldsymbol{R}_k}(C_e(\{\boldsymbol{R}_i\}, T_e'), \epsilon(T_e'))\, dT_e' \tag{A2}$$

$$= -\int_0^{T_e} \frac{\partial w}{\partial C_e}(C_e(\{\boldsymbol{R}_i\}, T_e'), \epsilon(T_e'))\frac{\partial^2 U}{\partial \boldsymbol{R}_k \partial T_e'}(\{\boldsymbol{R}_i\}, T_e')\, dT_e' \tag{A3}$$

$$\begin{aligned} = &-\frac{\partial w}{\partial C_e}(C_e(\{\boldsymbol{R}_i\}, T_e), \epsilon(T_e))\frac{\partial U}{\partial \boldsymbol{R}_k}(\{\boldsymbol{R}_i\}, T_e) \\ &+ \frac{\partial w}{\partial C_e}(C_e(\{\boldsymbol{R}_i\}, 0), \epsilon(0))\frac{\partial U}{\partial \boldsymbol{R}_k}(\{\boldsymbol{R}_i\}, 0) \\ &+ \int_0^{T_e} \frac{\partial^2 w}{\partial T_e' \partial C_e}(C_e(\{\boldsymbol{R}_i\}, T_e'), \epsilon(T_e'))\frac{\partial U}{\partial \boldsymbol{R}_k}(\{\boldsymbol{R}_i\}, T_e')\, dT_e' \end{aligned} \tag{A4}$$

where partial integration has been applied to Eq. (A3) to obtain Eq. (A4). If we assume $\partial U/\partial T_e(T_e = 0) \equiv 0$ then $C_e(\{\boldsymbol{R}_i\}, 0) = dE_e/dT_e(0)$ which is greater than or equal to $f\epsilon(0)$ per Eq. (14). It then follows from Eq. (12) and the differentiability of w that $\partial w/\partial C_e(T_e = 0) \equiv 0$ and thus the second term in Eq. (A4) is zero, giving rise to the expression for the auxiliary forces given in Eq. (10).

Appendix B: T_e-dependent silicon force field in full

Here we assemble the T_e-dependent silicon force field presented in this paper, including all of the functions and parameters, except for the functions $A(T_e)$, $B(T_e)$, and $\lambda(T_e)$, which are provided as tabulations in the Supplemental Material[66].

The equations that collectively define the T_e-dependent interatomic potential U are as follows:

$$U(\{\boldsymbol{R}_i\},T_e) = \frac{1}{2}\sum_{i\neq j} f_c(r_{ij})(A(T_e)e^{-\lambda_1 r_{ij}} - b_{ij}(\{\boldsymbol{R}_i\},T_e)B(T_e)e^{-\lambda_2 r_{ij}}), \tag{B1}$$

$$b_{ij}(\{\boldsymbol{R}_i\},T_e) = (1+\zeta_{ij}(\{\boldsymbol{R}_i\},T_e)^{\eta})^{-\delta}, \tag{B2}$$

$$\zeta_{ij}(\{\boldsymbol{R}_i\},T_e) = \sum_{k\neq i,j} f_c(r_{ik})\left[g(\theta_{ijk}) - \Lambda(g(\theta_{ijk}) - g_0, \lambda(T_e))\right] e^{\alpha(r_{ij}-r_{ik})^{\beta}}, \tag{B3}$$

$$g_0 = g(\cos^{-1}(-1/3)), \tag{B4}$$

$$g(\theta) = c_1 + \frac{c_2(h-\cos\theta)^2}{c_3+(h-\cos\theta)^2}\left(1+c_4 e^{-c_5(h-\cos\theta)^2}\right), \tag{B5}$$

$$\Lambda(x, y\geq 0) = \mathrm{sgn}(x)\begin{cases} |x| & |x|\leq y/\sqrt{2} \\ \sqrt{y^2-(y\sqrt{2}-|x|)^2} & y/\sqrt{2}<|x|<y\sqrt{2} \\ y & |x|\geq y\sqrt{2} \end{cases}, \tag{B6}$$

$$f_c(r) = \begin{cases} 1 & r\leq R_1 \\ \frac{1}{2}+\frac{9}{16}\cos\left(\pi\frac{r-R_1}{R_2-R_1}\right) - \frac{1}{16}\cos\left(3\pi\frac{r-R_1}{R_2-R_1}\right) & R_1<r<R_2 \\ 0 & r\geq R_2 \end{cases}. \tag{B7}$$

A general description of this force field can be found in Section III. The value of each parameter is provided in Table I, where the values were taken from [53] except for R_1, R_2, and α which were taken from [33].

Also required to apply our 2T-MD model is the Langevin damping parameter $\gamma = 1$ g/mol/ps, which determines the electron-phonon coupling rate; a lower bound on the electronic heat capacity for which we use $\epsilon(T_e) = \frac{1}{7}\frac{dE_e}{dT_e}(T_e)$; and the following function for the electronic energy $E_e(T_e)$ was obtained by fitting to the *ab initio* data:

$$E_e(T_e) = (10^{-3})T_e + (1.05125)T_e^2 + (0.0770416)T_e^4 \tag{B8}$$

where T_e is assumed to be in units of eV, and E_e has units of eV/atom.

Parameter	Value
λ_1 (Å^{-1})	3.2300135
λ_2 (Å^{-1})	1.3457970
η	1
δ	0.53298909
α	1.9
β	1
c_1	0.20173476
c_2	730418.72
c_3	1000000
c_4	1
c_5	26
h	−0.365
R_1 (Å)	3.1
R_2 (Å)	3.4

TABLE I: The force field parameters employed in this work, taken from Refs [33, 53]. The parameters A, B and λ are provided as T_e-dependent tabulations in the Supplemental Material[66].

Appendix C: Simulation of laser-irradiated nanofilms

The simulations in this paper are intended to reproduce the system studied experimentally by Harb et al. [1, 2] which involved 50 nm thick Si nanofilms irradiated with a single ultrafast optical pulse. The pulse had a spot size of 230 μm and a temporal full width at half maximum (FWHM) of 150 fs.

We model this setup using two-temperature molecular dynamics, the theoretical details of which are presented in Section IIA. Our simulation cell consists of a $50\times50\times92$ silicon lattice composed of $1,840,000$ atoms, with a lattice parameter of 5.431 Å. The cell is periodic only in the xy-plane so as to represent a 50 nm thick nanofilm that extends infinitely laterally. The nuclei and electrons are equilibrated at 300 K, after which the configuration is integrated in the microcanonical ensemble.

The laser pulse is delivered with a Gaussian temporal profile and is assumed to excite the crystal uniformly. This is justified by the following observations: The experimental probe observes a smaller spot size than the pulse, and on the picosecond timescale, there will be negligible lateral thermal diffusion over the $\sim 10^2$ μm length scale. Regarding the deposition as a function of depth, previous modelling [26] of silicon nanofilm irradiation that accounts for the temperature-dependence of the optical properties indicates a near-uniform excitation within the first 50 nm. In our model, the energy is delivered to the electrons via the heat source Q in the electronic heat

equation (4),

$$Q(t) = \frac{\Phi}{t_p h}\sqrt{\frac{4\log 2}{\pi}}\exp(-4\log 2(t-t_0)^2/t_p^2), \quad \text{(C1)}$$

where Φ is the absorbed fluence, h is the thickness of the nanofilm, t_0 is the time at which the pulse is at a maximum, and t_p is the FWHM.

The method, including the T_e-dependent force field, has been implemented into an in-house LAMMPS [67] package which is available upon request.

[1] M. Harb, R. Ernstorfer, T. Dartigalongue, C. T. Hebeisen, R. E. Jordan, and R. D. Miller, The Journal of Physical Chemistry B **110**, 25308 (2006).
[2] M. Harb, R. Ernstorfer, C. T. Hebeisen, G. Sciaini, W. Peng, T. Dartigalongue, M. A. Eriksson, M. G. Lagally, S. G. Kruglik, and R. D. Miller, Physical review letters **100**, 155504 (2008).
[3] S. Sundaram and E. Mazur, Nature materials **1**, 217 (2002).
[4] C. Shank, R. Yen, and C. Hirlimann, Physical Review Letters **50**, 454 (1983).
[5] H. W. Tom, G. Aumiller, and C. Brito-Cruz, Physical review letters **60**, 1438 (1988).
[6] J. Van Vechten, R. Tsu, and F. Saris, Physics Letters A **74**, 422 (1979).
[7] C. W. Siders, A. Cavalleri, K. Sokolowski-Tinten, C. Toth, T. Guo, M. Kammler, M. H. Von Hoegen, K. R. Wilson, D. von der Linde, and C. P. Barty, Science **286**, 1340 (1999).
[8] A. Cavalleri, C. Siders, F. Brown, D. Leitner, C. Toth, J. Squier, C. Barty, K. Wilson, K. Sokolowski-Tinten, M. H. Von Hoegen, *et al.*, Physical review letters **85**, 586 (2000).
[9] K. Sokolowski-Tinten, J. Bialkowski, and D. von der Linde, Physical Review B **51**, 14186 (1995).
[10] A. Lindenberg, I. Kang, S. L. Johnson, T. Missalla, P. Heimann, Z. Chang, J. Larsson, P. Bucksbaum, H. Kapteyn, H. Padmore, *et al.*, Physical review letters **84**, 111 (2000).
[11] X.-B. Li, X. Liu, X. Liu, D. Han, Z. Zhang, X. Han, H.-B. Sun, and S. Zhang, Physical review letters **107**, 015501 (2011).
[12] K. Bennemann, Journal of Physics: Condensed Matter **23**, 073202 (2011).
[13] C. Lian, S. Zhang, and S. Meng, Physical Review B **94**, 184310 (2016).
[14] N. Medvedev, Z. Li, and B. Ziaja, Physical Review B **91**, 054113 (2015).
[15] T. Zier, E. S. Zijlstra, S. Krylow, and M. E. Garcia, Applied Physics A **123**, 625 (2017).
[16] V. Recoules, J. Clérouin, G. Zérah, P. Anglade, and S. Mazevet, Physical review letters **96**, 055503 (2006).
[17] P. L. Silvestrelli, A. Alavi, M. Parrinello, and D. Frenkel, Physical review letters **77**, 3149 (1996).
[18] P. L. Silvestrelli and M. Parrinello, Journal of applied physics **83**, 2478 (1998).
[19] T. Zier, E. S. Zijlstra, A. Kalitsov, I. Theodonis, and M. E. Garcia, Structural Dynamics **2**, 054101 (2015).
[20] T. Zier, E. S. Zijlstra, and M. E. Garcia, Applied Physics A **117**, 1 (2014).
[21] P. Stampfli and K. Bennemann, Physical Review B **42**, 7163 (1990).
[22] P. Stampfli and K. Bennemann, Physical Review B **49**, 7299 (1994).
[23] H. M. Van Driel, Physical Review B **35**, 8166 (1987).
[24] G. S. Khara, S. T. Murphy, S. L. Daraszewicz, and D. M. Duffy, Journal of Physics: Condensed Matter **28**, 395201 (2016).
[25] P. Lorazo, L. J. Lewis, and M. Meunier, Physical Review B **73**, 134108 (2006).
[26] V. Lipp, B. Rethfeld, M. Garcia, and D. Ivanov, Physical Review B **90**, 245306 (2014).
[27] A. Rämer, O. Osmani, and B. Rethfeld, Journal of Applied Physics **116**, 053508 (2014).
[28] Y. Gan and J. Chen, Applied Physics A **105**, 427 (2011).
[29] D. Korfiatis, K. T. Thoma, and J. Vardaxoglou, Journal of Physics D: Applied Physics **40**, 6803 (2007).
[30] R. Darkins and D. M. Duffy, Computational Materials Science **147**, 145 (2018).
[31] K. Bennemann, Journal of Physics: Condensed Matter **16**, R995 (2004).
[32] L. Shokeen and P. K. Schelling, Applied Physics Letters **97**, 151907 (2010).
[33] L. Shokeen and P. K. Schelling, Journal of Applied Physics **109**, 073503 (2011).
[34] L. Shokeen and P. K. Schelling, Computational Materials Science **67**, 316 (2013).
[35] S. Khakshouri, D. Alfe, and D. Duffy, Physical Review B **78**, 224304 (2008).
[36] S. T. Murphy, S. L. Daraszewicz, Y. Giret, M. Watkins, A. L. Shluger, K. Tanimura, and D. M. Duffy, Physical Review B **92**, 134110 (2015).
[37] G. Norman, S. Starikov, and V. Stegailov, Journal of Experimental and Theoretical Physics **114**, 792 (2012).
[38] J. A. Moriarty, R. Q. Hood, and L. H. Yang, Physical review letters **108**, 036401 (2012).
[39] M. Weinert and J. Davenport, Physical Review B **45**, 13709 (1992).
[40] R. M. Wentzcovitch, J. L. Martins, and P. B. Allen, Physical Review B **45**, 11372 (1992).
[41] V. Lipp, D. Ivanov, B. Rethfeld, and M. Garcia, Journal of Optical Technology **81**, 254 (2014).
[42] S. Chandrasekhar, Reviews of modern physics **15**, 1 (1943).
[43] R. Kubo, Reports on progress in physics **29**, 255 (1966).
[44] W. T. Coffey, Y. P. Kalmykov, and J. Waldron, Chemistry and Electrical Engineering. World Scientific (2004).
[45] A. Rutherford and D. Duffy, Journal of Physics: Condensed Matter **19**, 496201 (2007).
[46] P.-W. Ma, S. Dudarev, and C. Woo, Physical Review B **85**, 184301 (2012).
[47] K. Furutsu, J. Res. Natl. Bur. Stand., Sect. D **67**, 303 (1963).
[48] E. A. Novikov, Sov. Phys. JETP **20**, 1290 (1965).
[49] I. Cook, Plasma Physics **20**, 349 (1978).
[50] C. L. Phillips and P. S. Crozier, The Journal of chemical

physics **131**, 074701 (2009).
[51] N. Hatano and M. Suzuki, in *Quantum annealing and other optimization methods* (Springer, 2005) pp. 37–68.
[52] G. Tsibidis, M. Barberoglou, P. Loukakos, E. Stratakis, and C. Fotakis, arXiv preprint arXiv:1007.5415 (2010).
[53] T. Kumagai, S. Izumi, S. Hara, and S. Sakai, Computational materials science **39**, 457 (2007).
[54] J. Tersoff, Physical Review B **38**, 9902 (1988).
[55] G. P. Pun and Y. Mishin, Physical Review B **95**, 224103 (2017).
[56] P. K. Schelling, Computational Materials Science **44**, 274 (2008).
[57] G. Kresse and J. Hafner, Physical Review B **47**, 558 (1993).
[58] G. Kresse and J. Hafner, Physical Review B **49**, 14251 (1994).
[59] G. Kresse and J. Furthmüller, Computational materials science **6**, 15 (1996).
[60] G. Kresse, Phys. Rev. B **54**, 11169 (1996).
[61] N. D. Mermin, Physical Review **137**, A1441 (1965).
[62] Y. Zhao and D. G. Truhlar, The Journal of chemical physics **125**, 194101 (2006).
[63] Y. Zhao and D. G. Truhlar, The Journal of chemical physics **130**, 074103 (2009).
[64] J. W. Precker and M. A. da Silva, American Journal of Physics **70**, 1150 (2002).
[65] J. P. Perdew, K. Burke, and M. Ernzerhof, Physical review letters **77**, 3865 (1996).
[66] See Supplemental Material at [URL] for a tabulation file containing the dependence of A, B, and λ on T_e.
[67] S. Plimpton, Journal of computational physics **117**, 1 (1995).